Hindawi
Journal of Nanomaterials
Volume 2021, Article ID 9716897, 11 pages
https://doi.org/10.1155/2021/9716897

Research Article

A Novel Fe_3O_4/Graphene Oxide Composite Prepared by Click Chemistry for High-Efficiency Removal of Congo Red from Water

Hongliu Jiang,[1] **Yao Cao**,[1] **Fengtao Zeng**,[2] **Zewu Xie**,[2] **and Fuan He**[2]

[1]*School of Materials Science and Engineering, Nanchang Hangkong University, Nanchang 330069, China*
[2]*School of Materials Science and Engineering, Guangdong University of Petrochemical Technology, Maoming 525000, China*

Correspondence should be addressed to Fuan He; he-fu-an@163.com

Received 25 July 2020; Revised 7 December 2020; Accepted 4 February 2021; Published 24 February 2021

Academic Editor: Thathan Premkumar

In this paper, a magnetic graphene oxide (MGO) composite was prepared by the click reaction between the alkyne-modified Fe_3O_4 nanoparticles and the azide-modified graphene oxide for the purpose of removing the Congo red (CR) dye from water. The deposition of the Fe_3O_4 nanoparticles on the graphene oxide to successfully prepare the MGO composite was evidenced by the Fourier-transform infrared spectrometer, wide-angle X-ray diffraction equipment, scanning electron microscope, thermal gravimetric analyzer, and Raman spectrometer. The value of saturation magnetization for the MGO composite was 34.9 emu/g. The CR absorption capacities of the MGO composite increased first and then decreased as the pH value increased. It was found that the maximum adsorption capacity of the MGO composite for the CR was as high as 769.2 mg/g. In the absorption-desorption experiment, the CR absorption capacities of the MGO composite from the second cycle to the fifth cycle remained stable to be about 130 mg/g. Moreover, both the Langmuir model for the adsorption isotherm and the pseudo-second-order kinetic model could be used to describe the CR absorption behaviors of the MGO composite.

1. Introduction

Recently, the problem of wastewater caused by organic dyes has aroused great concern and became an urgent event to be solved. So far, the commonly used technologies for the dye treatment of wastewater include biological treatment, coagulation/flocculation treatment, ozone treatment, chemical oxidation, membrane separation, and photocatalytic degradation [1–6]. Although the above methods have some advantages such as good decontamination ability, high efficiency, and convenient operation, they will consume enormous energy or have poor repeatability. For example, the degradation process needs not only exciting energy (e.g., gamma radiation or ultraviolet light) but also some additional chemicals (e.g., $S_2O_8^{2-}$ or/and H_2O_2) [7–9]. On the other hand, the adsorption method exhibited great potential for the treatment of wastewater containing various dyes [10–12]. Ahmed et al. have deposited magnesium/iron-layered double hydroxide nanoparticles on waste foundry sand. The adsorption capacity of the resultant composite for the Congo red (CR) dye reached as high as 9127.08 mg/g [10]. Zubair et al. have prepared the starch-NiFe-layered double hydroxide composite by the coprecipitation method, which possessed a high adsorption capacity of 387.59 mg/g for the methyl orange dye [11].

Graphene is a new material with many excellent properties such as its huge surface area and the possession of a number of free π electrons, which can be used as a good adsorbent for some dyes [13–15]. As a graphene derivative, graphene oxide (GO) has a two-dimensional planar structure similar to that of the graphene. GO contains a number of functional groups including carboxyl, hydroxyl, and epoxy on its surface, making it has a wide application prospect in the field of adsorbents with good absorption ability [16]. Magnetic nanometal oxides have been extensively studied and applied in magnetic fluid, data storage, catalysis, biomedicine, and pollutant treatment [17]. Graphene combined with magnetic nanomaterial can be used as an adsorbent to treat wastewater contaminants and then easily separated from an aqueous solution under external magnetic field conditions. It has been reported that the above magnetic GO composites simultaneously have the characteristics of GO and the magnetic

property, which are new materials widely used in environmental treatment in recent years [18–24].

There are many methods for the preparation of magnetic graphene-based composites [25–36]. The chemical precipitation method has been reported on the preparation of the Fe_3O_4/GO composites [25, 26]. In addition, by using the hydrazine hydrate or the gas/liquid interface reaction, the Fe_3O_4/GO composites were also prepared [28, 29]. Moreover, the superparamagnetic Fe_3O_4 nanoparticles could be synthesized by the solvothermal method. Hence, the solvent thermal reduction is one of the most common methods to obtain the magnetic Fe_3O_4/GO composites [30–36]. In particular, in order to enhance the binding force of the Fe_3O_4 particles and the GO, the Fe_3O_4/GO composites could be formed by the covalent bonding [26].

"Click chemistry" is an advanced synthesis method discovered by Sharpless et al., which can complete the chemical synthesis of the molecules quickly and reliably by the conjunction of small units [37]. This synthesis method has mild experimental conditions and usually can be operated at room temperature. In recent years, the synthetic method is widely used in the functionalized biological drug, the modification of nanoparticle surface, the application of complex drugs, the magnetic nanocomposites, and so on [38–44].

In recent years, the adsorption behaviors of the graphene and its derivatives were extensively studied. Graphene and its derivatives have a remarkable adsorption capacity on methylene blue (MB), fluoride, and other substances [41–50]. Chen et al. prepared the GO by the solvothermal method for the absorption of the MB in the aqueous solution [44]. Leng et al. prepared the GO by the modified Hummers method and then used it to absorb the toxic metal ion antimony with a high adsorption rate of 99.5% [49]. The adsorption of GO and reduced GO (RGO) for the acridine orange dye was also investigated [49]. Furthermore, the research studies on the adsorption of the organic dyes by the low-dimensional magnetic carbon nanomaterials have been increased. The magnetic Fe_3O_4/GO composites were used to absorb the MB and CR dyes with the adsorption capacities of 190.14 mg/g and 140.79 mg/g, respectively [42]. The magnetic iron nanoparticles/graphene (Fe/G) composites were also prepared for the absorption of MB [43].

In the current work, we had prepared the alkynylated Fe_3O_4 nanoparticles and then used the click chemistry to effectively attach them onto the azide-modified GO surface for the fabrication of a novel magnetic graphene oxide (MGO) composite, as shown in Figure 1. The resultant MGO composite was characterized by the Fourier-transform infrared (FTIR) spectrometer, the wide-angle X-ray diffraction (WAXD) equipment, the Raman spectrometer, the vibrating sample magnetometer (VSM), the X-ray photoelectron spectrometer (XPS), the thermogravimetric analyzer (TGA), and the scanning electron microscope (SEM). Furthermore, the absorption behavior of the MGO composite for the CR dye was studied in detail.

2. Materials and Methods

2.1. Materials. Graphite (average particle size 48 μm), Fe_3O_4 nanoparticles, aminopropyltriethoxysilane (APTES) as a silane coupling agent, propiolic acid, dicyclohexylcarbodiimide (DCC), 4-dimethylaminopyridine (DMAP), propiolic acid, L-ascorbic acid sodium salt, copper (II) sulfate pentahydrate ($CuSO_4{\cdot}5H_2O$), and anhydrous *N*,*N*-dimethylformamide (DMF) were purchased from the Energy Chemical Company (China). N_3-Poly(ethylene glycol)-NH_2, namely, N_3-PEG-NH_2, was obtained from the Shanghai To Young Bio Company (China). Dichloromethane (CH_2Cl_2) further dried by calcium hydride, ethanol (CH_3CH_2OH), and methanol (CH_3OH) were purchased from the Xi-Long Chemical Company (China). The CR dye was purchased from the Aladdin Reagent Company (China).

2.2. Preparation of the MGO Composite by the Click Reaction

2.2.1. Preparation of N_3-PEG-NH_2-Functionalized Graphene Oxide (GO-N_3). 20 mg GO was well dispersed in 8 mL $SOCl_2$ and then stirred at 65°C for 24 h. After the excessive $SOCl_2$ was removed, the resulting $SOCl_2$-modified GO was dispersed in 10 mL anhydrous DMF by ultrasonication. Next, 0.58 g DCC, 30 mg DMAP, and 150 mg N_3-PEG-NH_2 were added into the above $SOCl_2$-modified GO/DMF dispersion under nitrogen. The resultant mixture was magnetically stirred at room temperature for 2 h and 60°C for 48 h. After the reaction was completed, the resultant GO-N_3 was thoroughly washed with deionized water and ethanol and finally dried under vacuum at 50°C overnight.

2.2.2. Preparation of Propiolic Acid-Functionalized Fe_3O_4 Nanoparticles (Alkyne-Fe_3O_4). The mixture of 60 mg Fe_3O_4, 20 mL toluene, and 1.5 mL APTES was mechanically stirred at room temperature for 5 h under the protection of nitrogen. The resultant APTES-modified Fe_3O_4 (Fe_3O_4-NH_2) nanoparticles were washed with C_2H_5OH and CH_2Cl_2. The mixture of the above as-prepared Fe_3O_4-NH_2 nanoparticles, 20 mL anhydrous CH_2Cl_2, 0.75 g DCC, 68 mg DMAP, and 0.43 g propiolic acid was mechanically stirred for 1 h under the protection of an ice bath. Next, after the removal of the ice bath, the reaction was further carried out for 24 h at room temperature. The resulting alkyne-Fe_3O_4 black solid was magnetically separated, washed with C_2H_5OH for several times, and dried at 50°C under vacuum for 12 h.

2.2.3. Preparation of the MGO Composite. 1 mg sodium ascorbate and 1 mg $CuSO_4{\cdot}5H_2O$ were added into the solution containing 10 mg alkyne-Fe_3O_4, 16 mg GO-N_3, 8 mL DMF, and 2 mL deionized water. The resulting mixture was mechanically stirred at 60°C for 24 h under the protection of nitrogen. The resulting MGO composite was magnetically separated, washed with C_2H_5OH for several times, and dried at 50°C under vacuum for 12 h.

2.3. Characterization Techniques. FTIR results were obtained from the Bruker Vertex 70 instrument. X-ray diffraction (XRD) measurements were carried out on a Bruker D8 ADVANCE equipment. SEM images were obtained from the Hitachi/SU8010 equipment. Raman spectra were obtained from an HORIBA Jobin-Yvon LabRAM spectrometer. TGA results were obtained from the PerkinElmer Diamond equipment. Ultraviolet and visible (UV-Vis) absorption spectra were obtained from a WFXX-26A UV-Vis

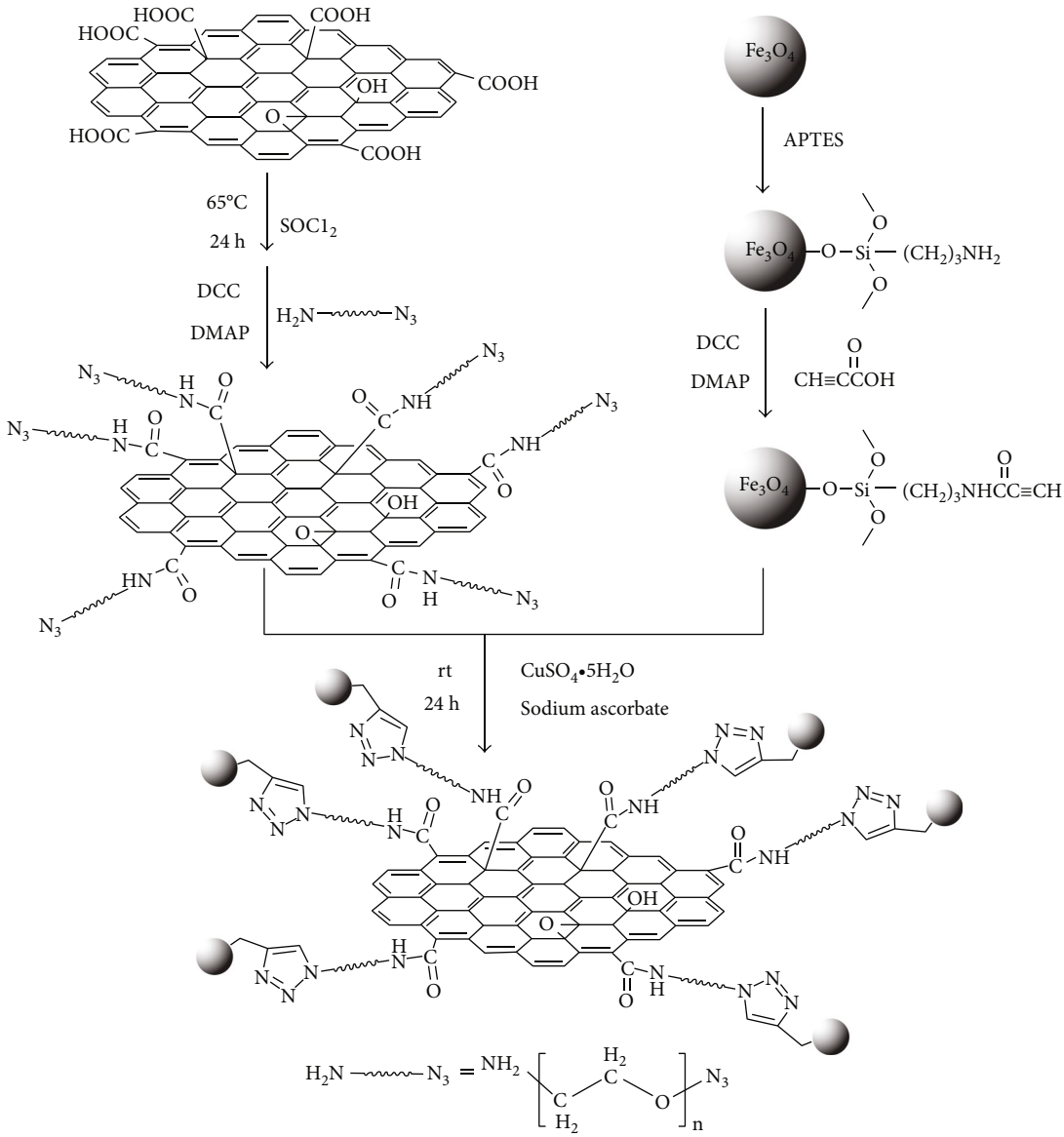

Figure 1: The synthesis route of the MGO composite.

spectrophotometer. The magnetic property was characterized using a VSM magnetic measuring instrument (Quantum Design, model MPMS, SQUID, US). XPS spectra were obtained from an X-ray photoelectron spectrometer in the Axis Ultra DLD model.

2.4. Adsorption Experiments. After the absorption by the MGO composite and the following separation of the MGO composite by a magnet, the equilibrium concentration (C_e) of the CR in the aqueous solution was measured with a UV-Vis spectrophotometer at the wavelength of 497 nm. The absorption capacity and the removal rate of the MGO composite for the CR were calculated by

$$q_t = \frac{(C_0 - C_e) \times V}{m},$$
$$R(\%) = \frac{C_0 - C_e}{C_0} \times 100, \quad (1)$$

where C_0 was the initial concentration of the CR in the aqueous solution before the absorption, V was the CR aqueous solution volume, and m was the MGO composite mass.

3. Results and Discussion

3.1. Characterization of the MGO Composite. It could be clearly observed from the SEM images of the MGO composite (see Figure 2) that a lot of Fe_3O_4 nanoparticles had been homogeneously attached on the surface of GO, which intuitively confirmed the formation of the magnetic Fe_3O_4/GO composite after the click reaction.

The FTIR spectra of the GO and the GO-N_3 are shown in Figure 3. The FTIR spectrum of the GO displayed the C=O stretching vibration of the carboxyl groups, the O-H stretching vibration of the hydroxyl groups in both the graphene skeleton and the carboxyl groups, the C=C stretching vibration of the graphene skeleton, and the C-O stretching

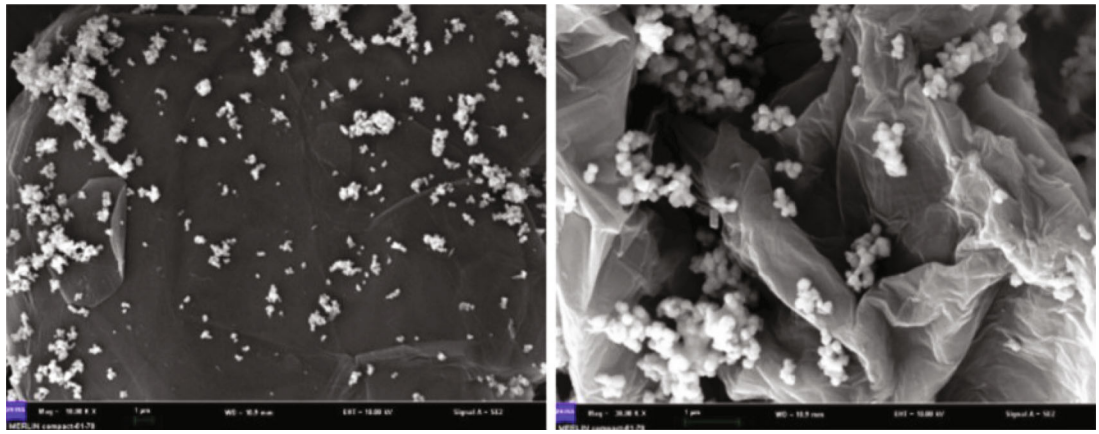

Figure 2: The SEM images of the MGO composite.

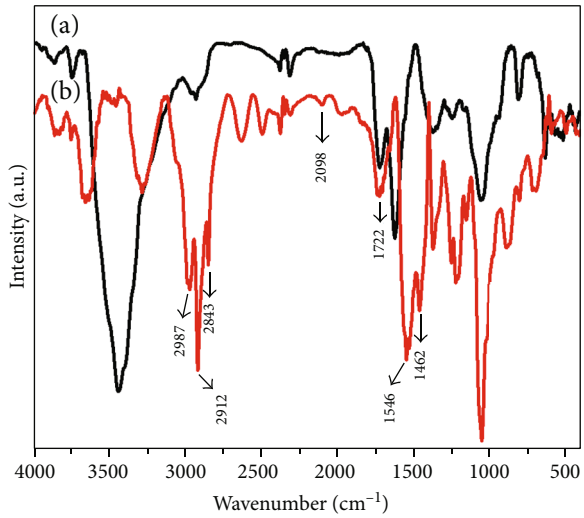

Figure 3: The FTIR spectra of (a) the GO and (b) the GO-N_3.

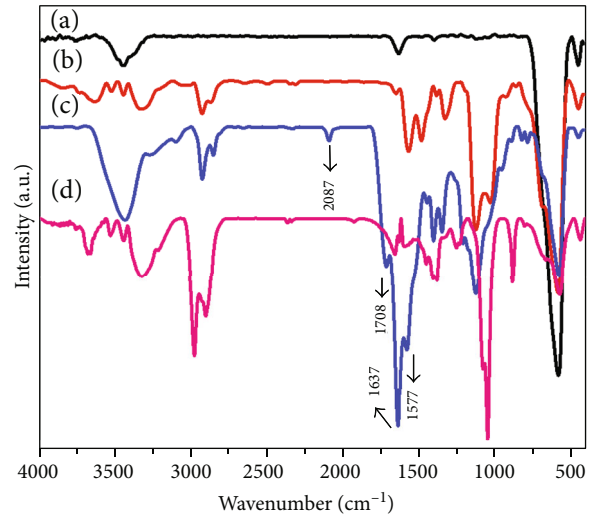

Figure 4: The FTIR spectra of (a) the Fe_3O_4 nanoparticles, (b) the Fe_3O_4-NH_2 nanoparticles, (c) the alkyne-Fe_3O_4 nanoparticles, and (d) the MGO composite.

vibration of the epoxy groups on the graphene skeleton at 1722 cm^{-1}, 3436 cm^{-1}, 1624 cm^{-1}, and 1062 cm^{-1}, respectively. After the modification of the GO, the resultant GO-N_3 exhibited a series of FTIR peaks at 1547 cm^{-1} for the N-H stretching vibration of the amide groups (band II), 1463 cm^{-1} for the C-N stretching vibration of the amide groups, 2912 cm^{-1} as well as 2843 cm^{-1} for the C-H stretching vibration of the methylene groups, and 2092 cm^{-1} for the N≡N stretching vibration of the azide groups, respectively. Moreover, compared with the FTIR spectrum of GO, both the higher peak intensity of the C-O stretching vibration for epoxy groups at 1052 cm^{-1} and the significantly decreased peak intensity of the O-H stretching vibration for carboxyl groups at 3436 cm^{-1} could be found in the FTIR spectrum of GO-N_3. These FTIR results confirmed the successful amidation reaction between the GO and the N_3-PEG-NH_2, indicating that the N_3-PEG-NH_2 macromolecules were linked to the GO by the covalent amide bonding.

The FTIR spectra of the Fe_3O_4 nanoparticles, the Fe_3O_4-NH_2 nanoparticles, the alkyne-Fe_3O_4 nanoparticles, and the MGO composite are shown in Figure 4. In the FTIR spectrum of the Fe_3O_4 nanoparticles, the peak at 582 cm^{-1} was related to the Fe-O stretching vibration and the other two peaks at 3443 cm^{-1} and 1631 cm^{-1} could be attributed to the hydroxyl groups on the surface of the Fe_3O_4 nanoparticles. In the FTIR spectrum of Fe_3O_4-NH_2 nanoparticles, the existence of a series of peaks at 1031 cm^{-1} for the Si-O stretching vibration, 1561 cm^{-1} for the N-H stretching vibration, and 2927 cm^{-1} along with 2867 cm^{-1} for the C-H stretching vibration indicated that the APTES had been successfully coated on the surface of Fe_3O_4 nanoparticles. After the further treatment of the Fe_3O_4-NH_2 nanoparticles with the propiolic acid, the resultant alkyne-Fe_3O_4 nanoparticles showed the characteristic FTIR peaks of the C=O stretching vibration of the amide groups, the N-H stretching vibration of the amide groups (band I as well as band II), the C-N stretching vibration of the amide groups, and the C≡C stretching vibration of alkynyl groups at 1712 cm^{-1}, 1638 cm^{-1}, 1585 cm^{-1}, 1448 cm^{-1}, and 2092 cm^{-1}, respectively. This indicated that the alkynyl functionalization of the Fe_3O_4 nanoparticles has been realized. After the click reaction between the GO-N_3 and the alkyne-Fe_3O_4, there were two characteristic peaks at

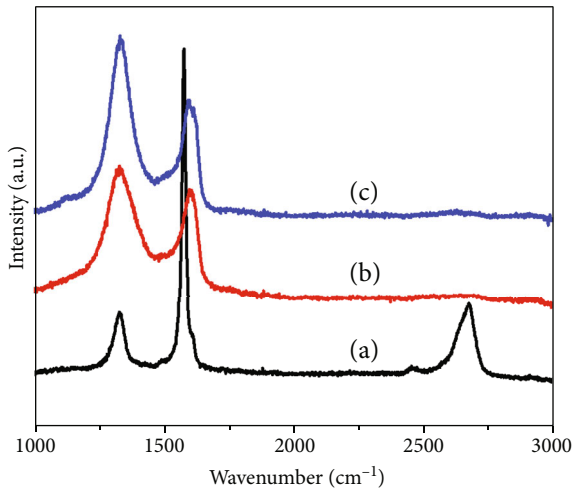

Figure 5: The Raman spectra of (a) the graphite, (b) the GO, and (c) the GO-N_3.

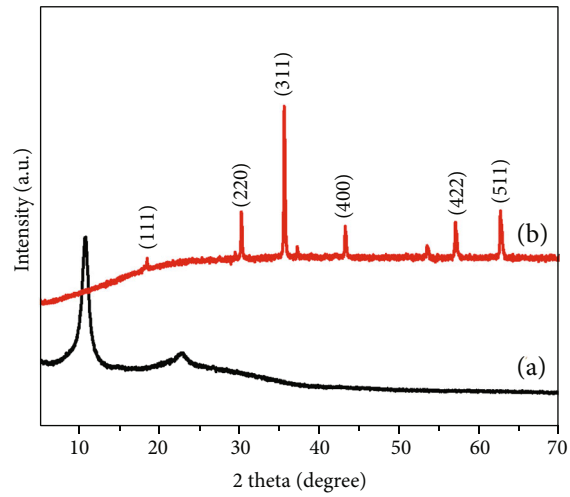

Figure 6: The WAXD patterns of the GO and the MGO composite.

580 cm^{-1} for the Fe-O stretching vibration and 880 cm^{-1} for the C-H stretching vibration of the benzene ring in the FTIR spectrum of the MGO composite, which proved the existence of both the Fe_3O_4 nanoparticles and the GO. Besides, it could also be found in the FTIR spectrum of the MGO composite that the characteristic peaks of the alkynyl groups at 2092 cm^{-1} and the azide groups at 2092 cm^{-1} disappeared and a new peak appeared at 1660 cm^{-1} for the triazole ring formed from the click reaction. This showed that the Fe_3O_4 nanoparticles have been covalently attached to the graphene by the click chemistry.

The Raman spectra of the graphite, the GO, and the GO-N_3 are shown in Figure 5. The Raman shifts of the D peak and the G peak for the graphite were at 1324 cm^{-1} and 1572 cm^{-1}, respectively, and the intensity ratio of the D peak to the G peak (I_d/I_g) for the graphite was 0.25. For the GO obtained from the oxidation of the graphite, its Raman shifts of the D peak and the G peak were at 1324 cm^{-1} and 1601 cm^{-1}, respectively, along with a I_d/I_g value of 1.36. These results indicated that there were many defections on the GO surface due to the breaking of carbon-carbon double bonds and the attachment of a lot of the oxygenating groups during the oxidation process. For the GO-N_3, its Raman shifts of the D peak and the G peak were at 1336 cm^{-1} and 1593 cm^{-1}, respectively, along with a I_d/I_g value of 1.48. This indicated that, after the grafting of the N_3-PEG-NH_2 on the graphene surface by the amidation reaction, the surface structure of the resultant GO-N_3 had been changed in comparison with that of the GO.

The WAXD patterns of the GO and the MGO composite are shown in Figure 6. In the WAXD pattern of the GO, the diffraction peak appearing at $2\theta = 10.6^\circ$ corresponded to the (001) crystal plane. In the WAXD pattern of the MGO composite, the (111), (220), (311), (400), (422), and (511) crystal planes of the Fe_3O_4 nanoparticles could be found at $2\theta =$ 18.27°, 30.1°, 35.4°, 43.05°, 56.94°, and 62.51°, respectively, indicating that the Fe_3O_4 nanoparticles were successfully loaded on the GO [51]. Moreover, the diffraction peaks of

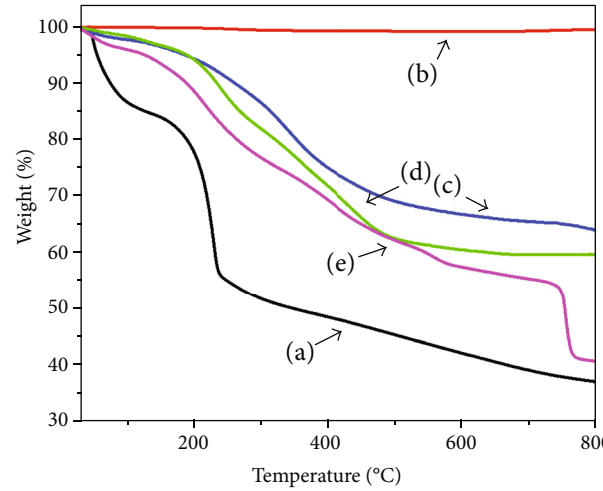

Figure 7: The TGA curves of (a) the GO, (b) the GO-N_3, (c) the Fe_3O_4 nanoparticles, (d) the Fe_3O_4-C≡C nanoparticles, and (e) the MGO composite.

the GO at $2\theta = 10.6^\circ$ disappeared in the MGO composite. It means that, by the incorporation of the Fe_3O_4 nanoparticles, the nanosheets of the GO in the MGO composite were in the exfoliated state without agglomeration.

The TGA curves of the GO, the GO-N_3, the Fe_3O_4 nanoparticles, the Fe_3O_4-C≡C nanoparticles, and the MGO composite under the argon atmosphere from room temperature to 800°C are shown in Figure 7. There were two significant weight loss stages in the TGA curve of the GO with a weight loss of 63.1 wt.% at 800°C. The first thermal decomposition stage of the GO below 100°C with a weight loss of 15.2 wt.% was mainly due to the evaporation of the adsorbed water while the second one between 150°C and 230°C with a weight loss of 29.6 wt.% could be ascribed to the decomposition of oxygen-containing functional groups. Similarly, the GO-N_3 also had two main thermal decomposition stages with a weight loss of 41.2 wt.% at 800°C and exhibited much more stability than the GO because the molecular weight of the

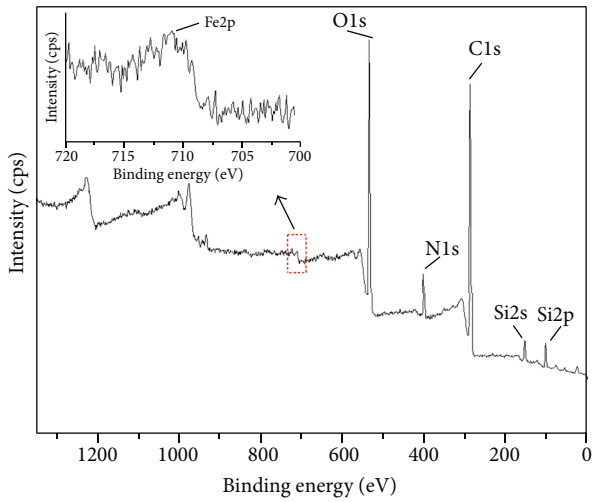

FIGURE 8: The XPS result of the MGO composite.

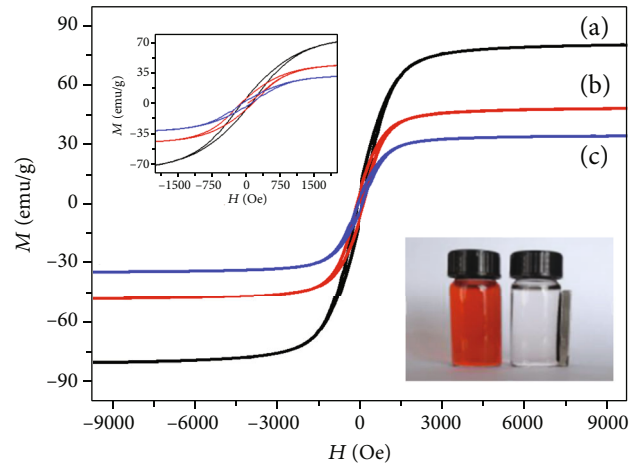

FIGURE 9: The magnetic properties of the pristine Fe_3O_4 nanoparticles and the MGO composite. Inset: the recollection of the MGO composite by a magnet after the CR absorption.

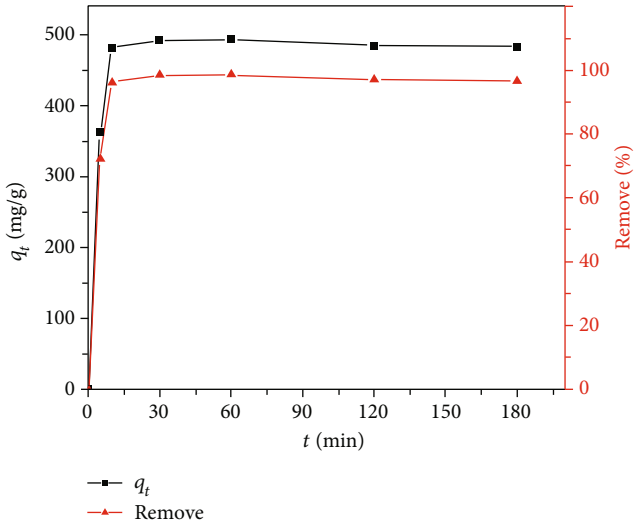

FIGURE 10: The relationship between the contact time and the absorption capacity of the MGO composite.

attached PEG chains was higher in comparison with the oxygen-containing functional groups. On the other hand, the pristine Fe_3O_4 nanoparticles only had a trace amount of weight loss at 800°C. After surface modification, the thermal stability of the resultant Fe_3O_4-C≡C nanoparticles was much lower than that of the pristine Fe_3O_4 nanoparticles with a weight loss of 59.2 wt.% at 800°C since there was a lot of organic component in it. In particular, the weight loss of the Fe_3O_4-C≡C nanoparticles occurred between 730°C and 780°C, which was probably caused by the breakage of the Si-O covalent bond between the silane coupling agent and the Fe_3O_4 nanoparticles. It was interesting that the thermal stability of the MGO composite obtained from click reaction was higher than that of the reactants including Fe_3O_4-C≡C nanoparticles and GO-N_3 with a weight loss of 46.0 wt.% at 800°C. Such a weight loss of the MGO composite could be attributed to the different components originating from the N_3-PEG-NH_2, the propiolic acid, the GO, and the silane coupling agent.

The XPS result of the MGO composite is shown in Figure 8, exhibiting several characteristic peaks for various elements including Si_{2p} (102.8 eV) as well as Si_{2s} (154.0 eV), O_{1s} (531.7 eV), C_{1s} (284.9 eV), N_{1s} (400.6 eV), and Fe_{2p} (711.0 eV and 717.1 eV). The existence of these elements in the MGO composite could be attributed to the different components originating from the Fe_3O_4 nanoparticles, the GO, the N_3-PEG-NH_2, the APTES, and the propiolic acid.

The magnetic properties of the pristine Fe_3O_4 nanoparticles and the MGO composite were measured by VSM at room temperature. As shown in Figure 9, the coercivities of the pristine Fe_3O_4 nanoparticles and MGO composite were 114 Oe and 106 Oe, respectively, while the remanences of the pristine Fe_3O_4 nanoparticles and MGO composite were 6.4 emu/g and 3.4 emu/g, respectively. On the other hand, the values of saturation magnetization (M_s) for the pristine Fe_3O_4 nanoparticles and the MGO composite were 81.1 emu/g and 34.9 emu/g, respectively, proving the existence of the magnetic Fe_3O_4 nanoparticles in the MGO composite. It was reasonable that the M_s values of the MGO composite were significantly lower than those of the pristine Fe_3O_4 nanoparticles because the components of the GO and the modifiers in the MGO composite were nonmagnetic.

3.2. Adsorption Studies of the MGO Composite. According to the relationship between the contact time (t) and the absorption capacity within t minute (q_t) of the MGO composite (see Figure 10) at the t moment, the MOG composite quickly absorbed the CR dye in the aqueous solution in 10 minutes and the absorption equilibrium was reached within 30 minutes. The CR absorption capacity of the MGO composite at equilibrium (q_e) was about 490 mg/g with a removal rate of about 98%. We believed that the good CR absorption ability of the MGO composite could be explained by two reasons: (1) both the high-surface area MGO composite and the CR had the benzene ring structure, leading to the mutual attraction by the π-π interaction, and (2) the MGO composite containing the hydroxyl group and the imide group could

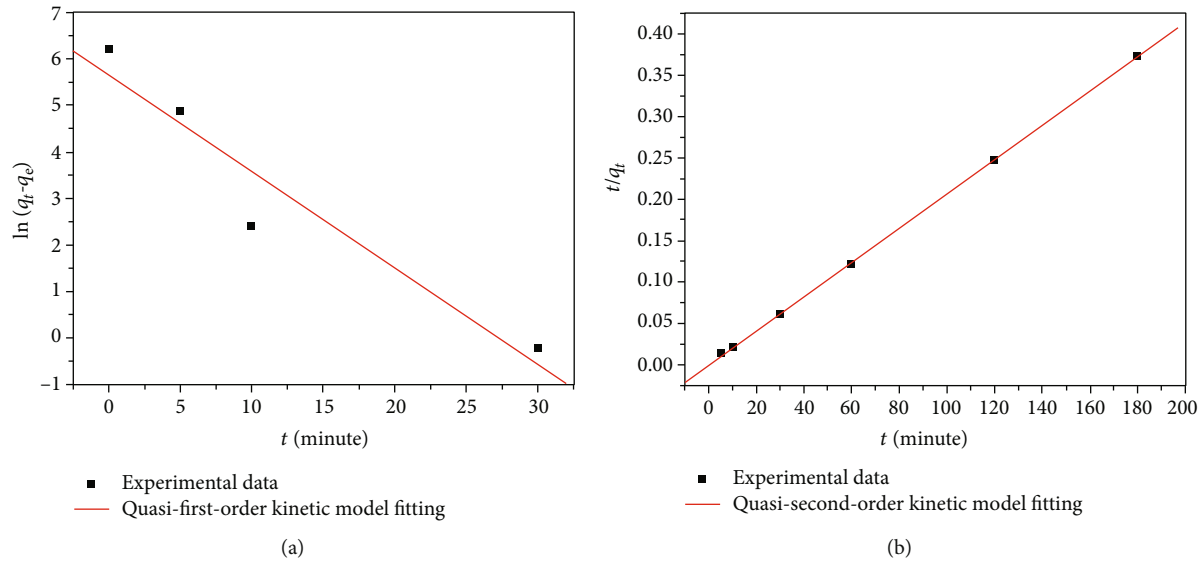

Figure 11: The experimental fitting results of the quasi-first-order kinetic model and the quasi-second-order kinetic model.

Table 1: Kinetic model fitting parameters of the MGO hybrid adsorb CR.

Pseudo-first-order kinetics		Pseudo-second-order kinetics	
$k_1 \times 10^{-3}$ g × mg^{-1} × min^{-1}	R^2	$k_2 \times 10^{-3}$ g × mg^{-1} × min^{-1}	R^2
0.3689	0.02565	0.1025	0.9998

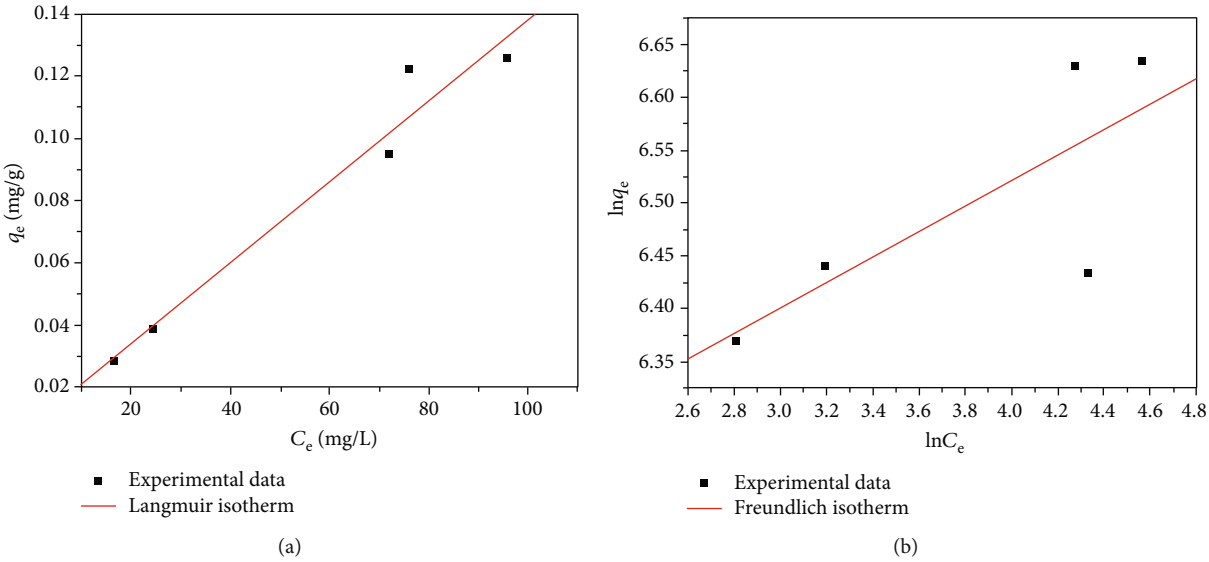

Figure 12: The experimental fitting results of the Langmuir isotherm model and the Freundlich isotherm model.

effectively absorb the CR containing the amine group by the hydrogen bonding and the dipole-dipole mutual interaction [52–55]. Moreover, the MGO composite after the CR absorption could be recollected by a magnet, as shown in the inset of Figure 9. Furthermore, the mechanism of the CR absorption kinetic model for the MGO composite was studied by the quasi-first-order model and the quasi-second-order model by the fitting of the t and the q_t as follows.

Table 2: Adsorption isotherm parameters for CR adsorption on the MGO hybrid composite.

Langmuir isotherm			Freundlich isotherm		
b (L/mg)	q_{mL} (mg/g)	R^2	K_f	n	R^2
0.164	769.2	0.949	418.857	0.121	0.459

Quasi-first-order kinetic model:

$$\ln (q_e - q_t) = \ln q_e - \frac{k_1 t}{2.303}. \quad (2)$$

Quasi-second-order kinetic model:

$$\frac{t}{q_t} = \frac{1}{k_2 q_e^2} + \frac{t}{q_e}, \quad (3)$$

where k_1 and k_2 were the constant. The experimental fitting results (see Figure 11 and Table 1) showed that the CR adsorption process of the MGO composite could be well fitted by the quasi-second-order kinetic model with $R^2 = 0.9998$, indicating that the CR adsorption kinetic model of the MGO composite was accurately simulated by the quasi-second-order kinetic model.

Both the Langmuir isotherm model (see Equation (4)) and the Freundlich isotherm model (see Equation (5)) were used to study the absorption isotherm of the MGO composite for the CR.

Langmuir isotherm model:

$$\frac{C_e}{q_e} = \frac{1}{bq_{mL}} + \frac{C_e}{q_{mL}}. \quad (4)$$

Freundlich isotherm model:

$$\ln q_e = \ln K_f + \frac{1}{n} \ln C_e, \quad (5)$$

where both b and K_f were the constant, and q_{mL} was the maximum CR absorption capacity of the MGO composite basing on the Langmuir isotherm model. As shown in Figure 12 and listed in Table 2, the adsorption process of the MGO composite was more consistent with the uniform monolayer CR adsorption described by the Langmuir model with the $R^2 = 0.949$. The q_{mL} value was calculated to be 769.2 mg/g, which was much higher than many other reported absorbents (see Table 3) [54–60].

Figure 13 shows the effect of the pH value on the CR absorption capacities of the MGO composite, which increased first and then decreased as the pH value increased. It is well known that the concentration of the H^+ decreases as the pH value increases. When the pH value was low, there was a competition between the protonated positive CR molecules and there was a lot of H^+ on the active adsorption site of the negative MGO composite. On the other hand, when the pH value was high, the CR became negatively charged, which resulted in the reduction of the mutual interaction with the negative MGO composite. Therefore, the maximum CR absorption capacity by the MGO composite could be obtained at pH = 7 with the maximum CR absorption capacity of 442.8 mg/g and the removal rate of 88.6%.

The MGO composite was subjected to the absorption-desorption experiment for the CR in five cycles (see Figure 14), and the resultant CR absorption capacities of the MGO composite were 442.8 mg/g with the removal rate of 88.6%, 133.3 mg/g with the removal rate of 26.7%, 128.9 mg/g with the removal rate of 25.8%, 137.7 mg/g with the removal rate of 27.5%, and 122.7 mg/g with the removal rate of 24.5% in sequence. This result was probably caused

Table 3: Maximum adsorption capacities of various adsorbents for CR.

Adsorbents	q_{max} (mg/g)	Ref.
Fe_3O_4/GO composite	113.2	[54]
Fe_3O_4/GO composite	33.66	[55]
GO/Fe_3O_4/PEI composite	575	[56]
MgO-GO composite	237	[57]
Fe_2O_3-Al_2O_3 composites	498	[58]
Fe_3O_4-TSPED-tryptophan	183.15	[59]
Fe_2O_3/sepiolite composites	126.4	[60]
MGO composite	769.2	This work

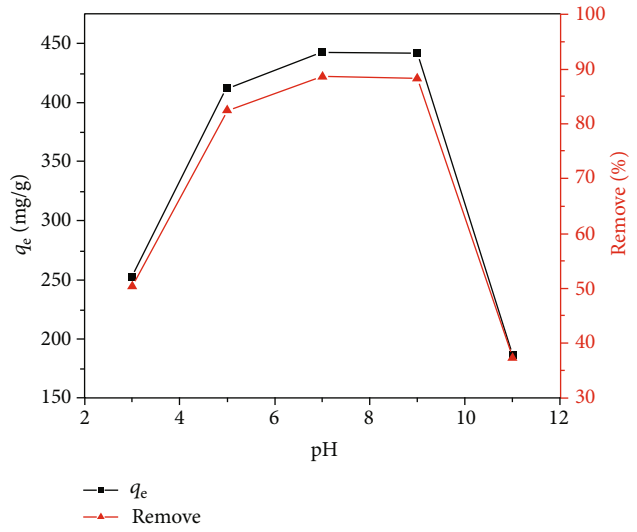

Figure 13: The effect of the pH value on the CR absorption performance of the MGO composite.

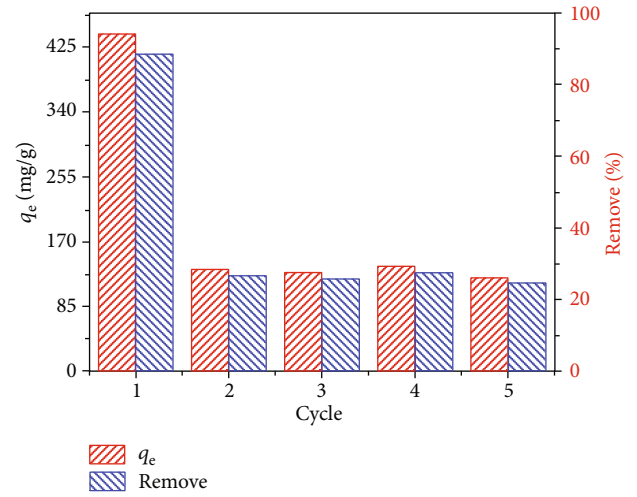

Figure 14: The absorption-desorption experiment result of the MGO composite for the CR in five cycles.

by the strong mutual interaction between some absorption sites of the MGO composite and the absorbed CR molecules, which were difficult to desorb. Although the regenerated ability of the MGO composite for the CR absorption was not ideal, the CR absorption capacities of the MGO composite from the second cycle to the fifth cycle remained stable to be about 130 mg/g. These values were still obviously higher than those (113.2 mg/g and 33.66 mg/g) of the other reported magnetic graphene-based absorbents [54–57].

4. Conclusion

Both the alkyne-modified Fe_3O_4 nanoparticles and the azide-modified GO were prepared and then attached together by the click chemistry to obtain the MGO composite. The successful attachment of the Fe_3O_4 nanoparticles onto the GO surface was testified by FTIR, WAXD, SEM, and Raman spectrum, and VSM. The optimized condition of the CR absorption by the MGO composite was at pH = 7. The MGO composite possessed a high CR absorption capacity of 769.2 mg/g and could be magnetically recollected after absorption. Moreover, the CR absorption behaviors of the MGO composite could be explained by the pseudo-second-order kinetic model and the Langmuir model. All of the experimental results indicated that the MGO composite could be a potential adsorbent to purify the wastewater containing the CR dye.

Data Availability

Any data used to support the findings of this study are available from the corresponding author upon request.

Conflicts of Interest

The authors declare that they have no conflicts of interest.

Acknowledgments

This work was financially supported by the NSFC (No. 51462024), the Natural Science Foundation of Jiangxi Province, China (No. 20151BAB203031), the Open Fund of Guangdong Provincial Key Laboratory of Petrochemical Pollution Process and Control for the Guangdong University of Petrochemical Technology, China (No. 2018B030322017), and the National Innovation and Entrepreneurship Training Program for College Students, China (Nos. 733286 and 733620).

References

[1] M. Kornaros and G. Lyberatos, "Biological treatment of wastewaters from a dye manufacturing company using a trickling filter," *Journal of Hazardous Materials*, vol. 136, no. 1, pp. 95–102, 2006.

[2] A. Lajeunesse, C. Gagnon, F. Gagné, S. Louis, P. Čejka, and S. Sauvé, "Distribution of antidepressants and their metabolites in brook trout exposed to municipal wastewaters before and after ozone treatment - evidence of biological effects," *Chemosphere*, vol. 83, no. 4, pp. 564–571, 2011.

[3] O. R. Gonzalez, F. Holzer, F. D. Kopinke, and A. Georgi, "Indications of the reactive species in a heterogeneous Fenton-like reaction using Fe-containing zeolite," *Applied Catalysis A: General*, vol. 398, no. 1-2, pp. 44–53, 2011.

[4] G. Capar, U. Yetis, and L. Yilmaz, "Membrane based strategies for the pre-treatment of acid dye bath wastewaters," *Journal of Hazardous Materials*, vol. 135, no. 1-3, pp. 423–430, 2006.

[5] Y. Ku, L. C. Wang, C. M. Ma, and Y. C. Chou, "Photocatalytic oxidation of Reactive Red 22 in aqueous solution using $La_2Ti_2O_7$ photocatalyst," *Water, Air, & Soil Pollution*, vol. 215, no. 1-4, pp. 97–103, 2011.

[6] A. B. Karim, B. Mounir, M. Hachkar, M. Bakasse, and A. Yaacoubi, "Removal of Basic Red 46dye from aqueous solution by adsorption onto Moroccan clay," *Journal of Hazardous Materials*, vol. 168, no. 1, pp. 304–309, 2009.

[7] M. Naushad, G. Sharma, and Z. A. Alothman, "Photodegradation of toxic dye using gum Arabic-crosslinked- poly(acrylamide)/$Ni(OH)_2$/FeOOH nanocomposites hydrogel," *Journal of Cleaner Production*, vol. 241, article 118263, 2019.

[8] N. S. Shaha, J. A. Khanb, M. Sayedb et al., "Synergistic effects of H_2O_2 and $S_2O_8^{2-}$ in the gamma radiation induced degradation of Congo-red dye: kinetics and toxicities evaluation," *Separation and Purification Technology*, vol. 233, article 115966, 2020.

[9] K. Balasubramani, N. Sivarajasekar, and M. Naushad, "Effective adsorption of antidiabetic pharmaceutical (metformin) from aqueous medium using graphene oxide nanoparticles: equilibrium and statistical modelling," *Journal of Molecular Liquids*, vol. 301, pp. 112–426, 2020.

[10] D. N. Ahmed, L. A. Naji, A. A. H. Faisal, N. Al-Ansari, and M. Naushad, "Waste foundry sand/MgFe-layered double hydroxides composite material for efficient removal of Congo red dye from aqueous solution," *Scientific Reports*, vol. 10, no. 1, article 2042, 2020.

[11] M. Zubair, N. Jarrah, A. K. Ihsanullah et al., "Starch-NiFe-layered double hydroxide composites: efficient removal of methyl orange from aqueous phase," *Journal of Molecular Liquids*, vol. 249, pp. 254–264, 2018.

[12] M. S. Samuel and S. Suman, "Venkateshkannan, E. Selvarajan, T. Mathimani, A. PugazhendhiImmobilization of Cu_3 $(btc)_2$ on graphene oxide-chitosan hybrid composite for the adsorption and photocatalytic degradation of methylene blue," *Journal of Photochemistry and Photobiology B: Biology*, vol. 204, pp. 111–809, 2020.

[13] K. S. Novoselov, V. I. Fal, L. Colombo, P. R. Gellert, M. G. Schwab, and K. Kim, "A road map for graphene," *Nature*, vol. 490, no. 7419, pp. 192–200, 2012.

[14] M. D. Stoller, S. Park, Y. Zhu, J. An, and R. S. Ruoff, "Graphene-based ultracapacitors," *Nano Letters*, vol. 8, no. 10, pp. 3498–3502, 2008.

[15] D. R. Dreyer, S. Park, C. W. Bielawski, and R. S. Ruoff, "The chemistry of graphene oxide," *Chemical Society Reviews*, vol. 39, no. 1, pp. 228–240, 2010.

[16] Y. Zhu, S. Murali, W. Cai et al., "Graphene and graphene oxide: synthesis, properties, and applications," *Advanced Materials*, vol. 22, no. 35, pp. 3906–3924, 2010.

[17] J. Chen, B. Yao, C. Li, and G. Shi, "An improved Hummers method for eco-friendly synthesis of graphene oxide," *Carbon*, vol. 64, pp. 225–229, 2013.

[18] Q. Wu, G. Zhao, C. Feng, C. Wang, and Z. Wang, "Preparation of a graphene-based magnetic nanocomposite for the

extraction of carbamate pesticides from environmental water samples," *Journal of Chromatography A*, vol. 1218, no. 44, pp. 7936–7942, 2011.

[19] G. Wang, Z. Gao, G. Wan, S. Lin, P. Yang, and Y. Qin, "High densities of magnetic nanoparticles supported on graphene fabricated by atomic layer deposition and their use as efficient synergistic microwave absorbers," *Nano Research*, vol. 7, no. 5, pp. 704–716, 2014.

[20] Q. Wu, M. Liu, X. Ma et al., "Extraction of phthalate esters from water and beverages using a graphene-based magnetic nanocomposite prior to their determination by HPLC," *Microchimica Acta*, vol. 177, no. 1-2, pp. 23–30, 2012.

[21] D. Sushanta, M. Arjun, and P. Kriveshini, "Impact of process parameters on removal of Congo red by graphene oxide from aqueous solution," *Journal of Environmental Chemical Engineering*, vol. 2, no. 1, pp. 260–272, 2014.

[22] Y. P. Chang, C. L. Ren, J. C. Qu, and X. G. Chen, "Preparation and characterization of Fe_3O_4/graphene nanocomposite and investigation of its adsorption performance for aniline and *p*-chloroaniline," *Applied Surface Science*, vol. 261, pp. 504–509, 2012.

[23] C. Wang, C. Feng, Y. Gao, X. Ma, Q. Wu, and Z. Wang, "Preparation of a graphene-basedmagnetic nanocomposite for the removal of an organic dye from aqueous solution," *Chemical Engineering Journal*, vol. 173, no. 1, pp. 92–97, 2011.

[24] G. Zhao, S. Song, C. Wang, Q. Wu, and Z. Wang, "Determination of triazine herbicides in environmental water samples by high-performance liquid chromatography using graphene-coated magnetic nanoparticles as adsorbent," *Analytica Chimica Acta*, vol. 708, no. 1-2, pp. 155–159, 2011.

[25] X. Yang, X. Zhang, Y. Ma, Y. Huang, Y. Wang, and Y. Chen, "Superparamagnetic graphene oxide–Fe_3O_4 nanoparticles hybrid for controlled targeted drug carriers," *Journal of Materials Chemistry*, vol. 19, no. 18, pp. 2710–2714, 2009.

[26] H. He and C. Gao, "Supraparamagnetic, conductive, and processable multifunctional graphenenanosheets coated with high-density Fe_3O_4 nanoparticles," *ACS Applied Materials & Interfaces*, vol. 2, no. 11, pp. 3201–3210, 2010.

[27] F. He, K. Lam, D. Ma, J. T. Fan, H. L. W. Chan, and L. M. Zhang, "Fabrication and characterization of graphene-Fe3O4 hybrids and syndiotactic polystyrene/graphene-Fe_3O_4 nanocomposites," *Carbon*, vol. 58, pp. 175–184, 2013.

[28] H. P. Cong, J. J. He, Y. Lu, and S. H. Yu, "Water-soluble magnetic-functionalized reduced graphene oxide sheets: in situ synthesis and magnetic resonance imaging applications," *Small*, vol. 6, no. 2, pp. 169–173, 2010.

[29] P. Lian, X. Zhu, H. Xiang, Z. Li, W. Yang, and H. Wang, "Enhanced cycling performance of Fe_3O_4-graphene nanocomposite as an anode material for lithium-ion batteries," *Electrochimica Acta*, vol. 56, no. 2, pp. 834–840, 2010.

[30] V. Chandra, J. Park, Y. Chun, J. W. Lee, I. C. Hwang, and K. S. Kim, "Water-dispersible magnetite reduced graphene oxide composites for arsenic removal," *ACS Nano*, vol. 4, no. 7, pp. 3979–3986, 2010.

[31] J. Liang, Y. Xu, D. Sui et al., "Flexible, magnetic, and electrically conductive graphene/Fe_3O_4 paper and its application for magnetic-controlled switches," *The Journal of Physical Chemistry C*, vol. 114, no. 41, pp. 17465–17471, 2010.

[32] H. Wang, J. T. Robinson, X. Li, and H. Dai, "Solvothermal reduction of chemically exfoliatedgraphene sheets," *Journal of the American Chemical Society*, vol. 131, no. 29, pp. 9910-9911, 2009.

[33] S. Dubin, S. Gilje, K. Wang et al., "A one-step, solvothermal reduction method for producing reduced graphene oxide dispersions in organic solvents," *ACS Nano*, vol. 4, no. 7, pp. 3845–3852, 2010.

[34] H. Deng, X. Li, Q. Peng, X. Wang, J. Chen, and Y. Li, "Monodisperse magnetic single-crystal ferrite microspheres," *Angewandte Chemie*, vol. 117, no. 18, pp. 2842–2845, 2005.

[35] Y. Zhan, F. Meng, X. Yang, and X. Liu, "Magnetite-graphene nanosheets (GNs)/poly(arylene ether nitrile) (PEN): Fabrication and characterization of a multifunctional nanocomposite film," *Colloids and Surfaces A: Physicochemical and Engineering Aspects*, vol. 390, no. 1-3, pp. 112–119, 2011.

[36] C. Hou, Q. Zhang, M. Zhu, Y. Li, and H. Wang, "One-step synthesis of magnetically-functionalized reduced graphite sheets and their use in hydrogels," *Carbon*, vol. 49, no. 1, pp. 47–53, 2011.

[37] H. C. Kolb, M. G. Finn, and K. B. Sharpless, "Click chemistry: diverse chemical function from a few good reactions," *Angewandte Chemie International Edition*, vol. 40, no. 11, pp. 2004–2021, 2001.

[38] H. N. Nagesh, N. Suresh, G. V. S. B. Prakash, S. Gupta, J. V. Rao, and K. V. G. C. Sekhar, "Synthesis and biological evaluation of novel phenanthridinyl piperazine triazoles via click chemistry as anti-proliferative agents," *Medicinal Chemistry Research*, vol. 24, no. 2, pp. 523–532, 2015.

[39] N. Pahimanolis, U. Hippi, L. S. Johansson et al., "Surface functionalization of nanofibrillated cellulose using click-chemistry approach in aqueous media," *Cellulose*, vol. 18, no. 5, article 1201, 2011.

[40] W. Yuan, W. Huang, and H. Zou, "Synthesis and properties of CO2-responsive copolymer by the combination of reversible addition-fragmentation chain transfer polymerization and click chemistry," *Polymer Bulletin*, vol. 73, no. 8, pp. 2199–2210, 2016.

[41] M. Namvari and H. Namazi, "Clicking graphene oxide and Fe_3O_4 nanoparticles together: an efficient adsorbent to remove dyes from aqueous solutions," *International Journal of Environmental Science and Technology*, vol. 11, no. 6, pp. 1527–1536, 2014.

[42] N. Liao, Z. Liu, W. Zhang et al., "Preparation of a novel Fe_3O_4/graphene oxide hybrid for adsorptive removal of methylene blue from water," *Journal of Macromolecular Science, Part A*, vol. 53, no. 5, pp. 276–281, 2016.

[43] F. He, J. Fan, D. Ma, L. Zhang, C. Leung, and H. L. Chan, "The attachment of Fe_3O_4 nanoparticles to graphene oxide by covalent bonding," *Carbon*, vol. 48, no. 11, pp. 3139–3144, 2010.

[44] L. Ai, C. Zhang, and Z. Chen, "Removal of methylene blue from aqueous solution by asolvothermal-synthesized graphene/magnetite composite," *Journal of Hazardous Materials*, vol. 192, no. 3, pp. 1515–1524, 2011.

[45] T. Liu, Y. Li, Q. Du et al., "Adsorption of methylene blue from aqueous solution by graphene," *Colloids and Surfaces B: Biointerfaces*, vol. 90, pp. 197–203, 2012.

[46] T. Wu, X. Cai, S. Tan, H. Li, J. Liu, and W. Yang, "Adsorption characteristics of acrylonitrile, p-toluenesulfonic acid, 1-naphthalenesulfonic acid and methyl blue on graphene in aqueous solutions," *Chemical Engineering Journal*, vol. 173, no. 1, pp. 144–149, 2011.

[47] Y. Li, P. Zhang, Q. Du et al., "Adsorption of fluoride from aqueous solution by graphene," *Journal of Colloid and Interface Science*, vol. 363, no. 1, pp. 348–354, 2011.

[48] Y. Wang, S. Gao, X. Zang, J. Li, and J. Ma, "Graphene-based solid-phase extraction combined with flame atomic absorption spectrometry for a sensitive determination of trace amounts of lead in environmental water and vegetable samples," *Analytica Chimica Acta*, vol. 716, pp. 112–118, 2012.

[49] Y. Leng, W. Guo, S. Su, C. Yi, and L. Xing, "Removal of antimony(III) from aqueous solution by graphene as an adsorbent," *Chemical Engineering Journal*, vol. 211-212, pp. 406–411, 2012.

[50] L. Sun, H. Yu, and B. Fugetsu, "Graphene oxide adsorption enhanced by *in situ* reduction with sodium hydrosulfite to remove acridine orange from aqueous solution," *Journal of Hazardous Materials*, vol. 203-204, pp. 101–110, 2012.

[51] W. Wei, X. Yue, Y. Zhou et al., "New promising hybrid materials for electromagnetic interference shielding with improved stability and mechanical properties," *Physical Chemistry Chemical Physics*, vol. 15, no. 48, pp. 21043–21050, 2013.

[52] J. Gong, X. Wang, G. M. Zeng et al., "Copper (II) removal by pectin–iron oxide magnetic nanocomposite adsorbent," *Chemical Engineering Journal*, vol. 185-186, pp. 100–107, 2012.

[53] Y. Jiang, D. Chen, W. Yang, S. Wu, and X. Luo, "Reduced graphene oxide enhanced magnetic nanocomposites for removal of carbamazepine," *Journal of Materials Science*, vol. 53, no. 22, pp. 15474–15486, 2018.

[54] M. Namvari and H. Namazi, "Preparation of efficient magnetic biosorbents by clicking carbohydrates onto graphene oxide," *Journal of Materials Science*, vol. 50, no. 15, pp. 5348–5361, 2015.

[55] Y. Yao, S. Miao, and S. Liu, "Synthesis, characterization, and adsorption properties of magnetic Fe_3O_4@graphene nanocomposite," *Chemical Engineering Journal*, vol. 184, pp. 326–332, 2012.

[56] L. Wang, C. Mao, N. Sui, M. Liu, and W. Yu, "Graphene oxide/ferroferric oxide/polyethylenimine nanocomposites for Congo red adsorption from water," *Environmental Technology*, vol. 38, no. 8, pp. 996–1004, 2017.

[57] J. Xu, D. Xu, B. Zhu, B. Cheng, and C. Jiang, "Adsorptive removal of an anionic dye Congo red by flower-like hierarchical magnesium oxide (MgO)-graphene oxide composite microspheres," *Applied Surface Science*, vol. 435, pp. 1136–1142, 2018.

[58] A. Mahapatra, B. G. Mishra, and G. Hota, "Adsorptive removal of Congo red dye from wastewater by mixed iron oxide–alumina nanocomposites," *Ceramics International*, vol. 39, no. 5, pp. 5443–5451, 2013.

[59] K. S. Jitendra, K. P. Sanjeev, M. Monalisa, and S. Harekrushna, "Amine functionalized magnetic iron oxide nanoparticles: synthesis, antibacterial activity and rapid removal of Congo red dye," *Journal of Molecular Liquids*, vol. 282, pp. 428–440, 2019.

[60] Q. Wang, A. Tang, L. Zhong, X. Wen, P. Yan, and J. Wang, "Amino-modified γ-Fe_2O_3/sepiolite composite with rod-like morphology for magnetic separation removal of Congo red dye from aqueous solution," *Powder Technology*, vol. 339, pp. 872–881, 2018.